The Impact of Carbon Nanotube Length and Diameter on their Global Alignment by Dead-End Filtration

Christian Rust, Pavel Shapturenka, Manuel Spari, Qihao Jin, Han Li, Andreas Bacher, Markus Guttmann, Ming Zheng, Tehseen Adel, Angela R. Hight Walker, Jeffrey A. Fagan, and Benjamin S. Flavel*

Dead-end filtration has proven to effectively prepare macroscopically (3.8 cm^2) aligned thin films from solutionbased single-wall carbon nanotubes (SWCNTs). However, to make this technique broadly applicable, the role of SWCNT length and diameter must be understood. To date, most groups report the alignment of unsorted, large diameter (≈1.4 nm) SWCNTs, but systematic studies on their small diameter are rare (≈0.78 nm). In this work, films with an area of A = 3.81 cm^2 and a thickness of ≈40 nm are prepared from length-sorted fractions comprising of small and large diameter SWCNTs, respectively. The alignment is characterized by cross-polarized microscopy, scanning electron microscopy, absorption and Raman spectroscopy. For the longest fractions (L_{avg} = 952 nm ± 431 nm, Δ = 1.58 and L_{avg} = 667 nm ± 246 nm, Δ = 1.55), the 2D order parameter, S2D, values of ≈0.6 and ≈0.76 are reported for the small and large diameter SWCNTs over an area of A = 625 μm^2, respectively. A comparison of Derjaguin, Landau, Verwey, and Overbeek (DLVO) theory calculations with the aligned domain size is then used to propose a law identifying the required length of a carbon nanotube with a given diameter and zeta potential.

1. Introduction

The outstanding electronic, mechanical, thermal, and optical properties of single-wall carbon nanotubes (SWCNTs)[1] have led them to find applications across a broad range of fields. These encompass energy,[2] photonics,[3] electronics,[4] and medicine,[5]

but each requires the ability to control the location and orientation of individual SWCNTs and/or their organization in thin films. Correspondingly, and due to their highly anisotropic properties, researchers have developed various methods to form thin films with in-plane (axial) alignment. These include the dry shear of vertically grown forests and mis-aligned films,[6] the use of faceted nano-steps on a miscut sapphire surface to direct growth,[7] Langmuir–Blodgett deposition,[8] evaporation induced self-assembly,[9] the use of magnetic and electric fields,[10] the stretching of SWCNT-polymer matrices,[11] or the confined shear of nanotube dispersions.[12] However, it is the method described by He et al.[13] and in preliminary works by Shaffer et al.,[14] Dan et al.,[15] and King & Panchapakesan,[16] using dead-end filtration to deposit aligned SWCNT films that are particularly attractive. Filtration has been shown to not only afford wafer-scale films with a high packing density and high nematic order (conventionally described by the order parameter S$_{2D}$), but filtration is also compatible with solution-based separation techniques[2f,17] to select the diameter,[18] length,[19] wall-number,[20] electronic property,[21] species (often termed chirality),[22] and enantiomeric type[23] of the SWCNTs employed.

C. Rust, M. Spari, H. Li, B. S. Flavel
Institute of Nanotechnology
Karlsruhe Institute of Technology
Hermann-von-Helmholtz Platz 1
76344 Eggenstein-Leopoldshafen, Germany
E-mail: benjamin.flavel@kit.edu
C. Rust
Institute of Materials Science
Technische Universität Darmstadt
Alarich-Weiss-Straße 2, 64287 Darmstadt, Germany

The ORCID identification number(s) for the author(s) of this article can be found under https://doi.org/10.1002/smll.202206774.

P. Shapturenka, M. Zheng, J. A. Fagan
Materials Science and Engineering Division
National Institute of Standards and Technology
Gaithersburg, MD 20899, USA
Q. Jin
Light Technology Institute
Karlsruhe Institute of Technology
Engesserstraße 13, 76131 Karlsruhe, Germany
A. Bacher, M. Guttmann
Institute of Microstructure Technology
Karlsruhe Institute of Technology
Hermann-von-Helmholtz-Platz 1
76344 Eggenstein-Leopoldshafen, Germany
T. Adel, A. R. H. Walker
Quantum Measurement Division
National Institute of Standards and Technology
Gaithersburg, MD 20899, USA

With dead-end filtration, global alignment of SWCNTs has primarily been demonstrated for polyvinylpyrrolidone (PVP) coated polycarbonate track etched (PCTE) membranes filtering surfactant dispersed SWCNTs, but only when using a sequence of well-controlled flow rate conditions.[13,24] Although this appears straightforward, control of the initial volumetric flow rate, which must vary from 1 to ≈ 6 mL h^{-1}[13,25] with an accuracy of ± 25 µL min^{-1},[26] and other unknown parameters, have precluded the widespread use of this technique. It should be mentioned, that these values have to be always discussed in terms of the actual membrane area being used. These problems are amplified considering most research groups only have access to a standard bench-top filtration apparatus with a manual valve to control and regulate the volume rate. Furthermore, optimized volume rate conditions for the alignment of one batch of SWCNTs have proven not to be directly compatible with the next batch. For example, variations in the total mass; the concentration; and diameter of the SWCNTs to be filtered; the filtration area and pore size of the membrane; the zeta potential of both; and the surfactant used, have all been shown to affect the quality of alignment and/or determine if alignment will occur in the first place.[13,25–27] Evidently, for each SWCNT dispersion there is a narrow set of parameters that will lead to alignment, but an understanding of how each of these parameters influences each other, along with a complete description of the alignment mechanism is still required. As an example, He et al.[13,25] report large diameter ($d_t ≈ 1.4$ nm) SWCNTs to align better than their small diameter ($d_t ≈ 0.73$ to 1 nm) counterparts but it is unclear why and which experimental parameter(s) would lead to an improvement. This is also reflected by the multitude of studies on aligning large diameter electric arc synthesis method SWCNTs (EA-SWCNTs),[24a,25–28] while only a few studies can be found on small diameter cobalt-molybdenum catalyst synthesis method (CoMoCAT) SWCNTs.[13,29]

The authors of this paper have been involved in the development of several filtration setups that can control the flow rate with the required precision for SWCNT alignment. Walker et al.[25] built a parallelized setup in a vacuum filtration assembly using machine vision to identify the height of the SWCNT dispersion above the membrane and a feedback loop between the liquid height and the applied vacuum pressure difference to control the flow rate.[25] Alternatively, Rust et al.[26] built a positive pressure setup capable of in situ measurement of the transmembrane pressure (p_{TMP}), which is defined as the difference of pressure on the feed (p_{in}) and permeate (p_{out}) sides of the membrane. A feedback loop minimizing the error between the actual flow and the desired flow (setpoint) as measured by an inline Coriolis flow sensor was then used to control the inlet pressure p_{in} (process variable) and obtain a volume rate accuracy of ± 1.7 µL min^{-1} at 100 µL min^{-1}. Both methods enable monitoring, control, and optimization of the applied filtration flux for producing aligned films and variations for different solutions. However, the positive pressure setup with its direct measurement of flow rate and p_{TMP} also allows for more precise calculation of the membrane resistance with respect to the permeated volume, which in turn meant that the mode of fouling could be determined, or in other words, the manner in which mass accumulated on the membrane.[30]

Through measurement of the instantaneous membrane resistance during filtration, our previous work found that an increase in filtration resistance was essential for achieving films comprised of aligned SWCNTs. Either intermediate or cake fouling could be occurring on the membrane, but the best films were those prepared under conditions with a small critical permeate volume. The critical permeate volume is conventionally defined for dead-end filtration as the volume below which no fouling occurs, but eventually fouling is inevitable as mass accumulates at the membrane surface consistently[31] and the volume is known to decrease with increasing flow-rate.[31c] Hence, concentration polarization (CP) is the loose accumulation of mass above the surface of a membrane,[31b] and occurs, if the back diffusion of the SWCNTs and their total DLVO forces (Φ_{TOT}) counter the convection in the very beginning of the filtration.[32] In early work, He et al.[13] used the concepts of CP and suggested that SWCNTs self-orientate in a 2D plane of minimum potential above the surface of the membrane. This plane of minimum potential was described as the consequence of attractive van der Waals forces (Φ_{VDW}) and repulsive electric double-layer forces (Φ_{EDL}) being superimposed, or more specifically Φ_{TOT}. From our work, it is now known that an extended CP regime leads to the formation of large SWCNT domains/crystallites, but these are not globally aligned. We have speculated that there is an optimum flow-rate and CP volume,[26] that allows SWCNT to seed crystallites initially formed to further grow on the membrane surface. The full set of factors that lead to this growth and optimal global alignment of monodomains is still a topic of dispute. A popular hypothesis is that the SWCNTs domains experience a shared shear flow with an aligning direction defined by a series of micro and macro grooves in the membrane and that this acts to elongate and globally align the domains. Alternative explanations include those provided by Komatsu et al.,[24a,33] who proposed that global alignment is due to structural templating of the SWCNTs by the grooves, and that of Walker et al. who conclude that the grooves are not the primary source of alignment, but rather an underlying set of directional charge or colloidal interactions perhaps co-produced with the observed grooves during the roll-to-roll production process of the membranes.[25] Varied experiments have tested each of these hypotheses, but reaching definitive answers is challenging, and may contain combinations of multiple effects depending on the nanotube, membrane, and solution properties and the flow rate regime being applied. Independently evaluating the effects on filtration of two of the critical nanotube properties that can vary in different SWCNT populations, length and diameter, are the key purpose of this contribution.

SWCNT length and diameter are parameters that critically impact the global alignment process (vide infra). Filtration conditions previously identified as being optimal for electric arc EA-SWCNTs with an average length of ≈ 690 nm are applied to length sorted fractions of small (CoMoCAT) and large diameter EA-SWCNTs. Intuitively, longer SWCNTs will have greater absolute strength of van der Waals and other colloidal interactions, greater relative interactions as compared to the energy for Brownian motion, experience enhanced torque from directional force fields, and have a longer length scale for interacting with other particles. A downside of a longer length,

however, is a reduced rotational diffusivity, and a greater likelihood of entanglement out of the alignment direction with other SWCNTs; both factors would make it more difficult to rotate into a globally aligned direction. In previous literature, He et al. report an average SWCNT length of 227 nm, while Walker et al. state a distribution range of 200–400 nm.[27,46] In these works, the use of relatively short SWCNTs could be interpreted as the ability of the SWCNT to rotate being the most important parameter to global alignment, but it is difficult to draw a clear conclusion, especially in light of the comparatively long (690 & 845 nm) SWCNTs used by Rust et al.[26] In the current work, we use Derjaguin, Landau, Verwey, and Overbeek (DLVO) theory calculations utilized by McLean et al.[34] and recently refined by Wu et al.[35] to calculate the total interaction potential of each length sorted CNT with the PCTE membrane and use cross-polarized microscopy and machine vision to evaluate the size and shape of the crystallites formed. By comparing the experimental results with the secondary minima of the corresponding DLVO-calculations, we are able to formulate a rule, which defines the needed length for a given diameter and zeta-potential of a CNT in order to form domains with the necessary size to globally align.

2. Results and Discussion

SWCNT soot from the EA and CoMoCAT synthesis methods was used in this work. Both sets of SWCNTs were dispersed via tip sonication in surfactant solution, centrifuged to remove large aggregates, and sorted via a rate-zonal (RZ) centrifugation process to further remove bundled and morphologically impure SWCNTs (see Experimental Section for additional details). In the case of the EA-SWCNTs, the SWCNTs were also filled with a linear alkane, $C_{20}H_{42}$, prior to dispersion as previously reported,[36] and subjected to aqueous two-phase extraction (ATPE) after the RZ process to separate the metallic (m) and semiconducting (s) species from each other.[37] The EA-SWCNTs have an average diameter of ≈ 1.4 nm. The CoMoCAT samples as used for filtration were water-filled and contained

both metallic and semiconducting species. Neither aspect, we believe, is significant to the results of this effort; of importance is that these samples have an average SWCNT diameter of ≈ 0.78 nm. Both parent dispersions were separated by size exclusion chromatography (SEC) while dispersed in 10.0 g L^{-1} sodium deoxycholate (DOC) solution, generating fractionated populations with tightly constrained distributions of different average lengths.[38] A total of 12 fractions of sufficient concentration were obtained from the SEC column and alternate fractions were used in filtration experiments to minimize the length overlap. These were labeled A2, A4, A6, and A10 for the EA-SWCNTs and B2 and B4 for the CoMoCAT SWCNTs; in SEC the longest SWCNTs elute first, so the average length is longest for A2 and decreases with increasing fraction number. The average length of each was determined by atomic force microscopy (AFM) and analysis of the length-dependent sedimentation coefficient as measured by analytical ultracentrifugation (AUC), **Figure 1**A, Figure S1 and Figure S2 (A), Supporting Information. As expected for SEC, both AFM and AUC confirmed that the average SWCNT length (L_{avg}) increased with decreasing fraction number, with AFM reporting slightly longer average length values (direct number distribution counting) than those converted to apparent number distributions from the signal-weighted distribution measured by AUC. Due to its widespread use by other groups, the length values determined AFM will be taken throughout the remainder of this work and experiments with EA-SWCNTs will be discussed first.

The average lengths of the EA-SWCNT fractions were A2: 667 ± 246 nm, A4: 524 ± 178 nm, A6: 335 ± 131 nm, and A10: 60 ± 14 nm and there were no significant differences in the optical spectrum between each fraction as shown in Figure 1B. These length distributions are significantly narrower than any applied to prior aligned filtration studies. The high degree of semiconducting species purity and lack of impurities in the fractions used are also reflected in the clearly distinguishable SWCNT optical transitions and the very low background absorption of the absorbance spectra. The concentration of each fraction was evaluated as described previously,[26] using the absorbance of the π-plasmon peak after dilution by a factor
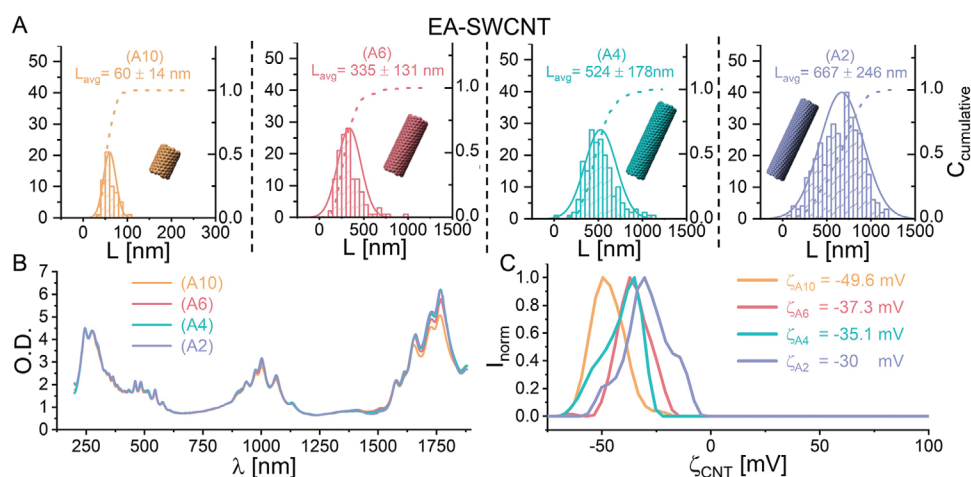

Figure 1. A) Length determination of the EA-SWCNT fractions by AFM analysis of individualized SWCNTs on a silicon wafer. B) Absorption spectra of the EA-SWCNT fractions. C) Zeta potential ζ_{SWCNT} measurements at a concentration of 8 µg mL^{-1} SWCNTs and 0.04 % DOC.

of 10 with deionized water (Figure S3, Supporting Information). Each fraction was adjusted to a SWCNT concentration of 8 µg mL^{-1}, dispersed in 0.4 g L^{-1} (0.04 %, $\approx$ 1 mmol L^{-1}) DOC and the zeta potential measured (Experimental Section), Figure 1C. The shorter SWCNTs were reported by the instrument to be slightly more charged than the longer SWCNTs (A10: −49.6 mV vs A2: −30 mV). This could be interpreted as a tendency of the surfactant to more densely cover shorter SWCNTs, however, the observed variation may also be due to deviations of the SWCNT sample from the geometric considerations embedded in the instrument's implementation of the Smoluchowski equation. Both the embedded consideration of the rod-shaped SWCNTs as spheres and the relative scale of the Debye length, $\approx$ 10 nm for a 1 mmol L^{-1} symmetric electrolyte,[39] to the diameter of the SWCNT plus its surfactant shell could affect the accuracy of the reported values. An increase in SWCNT length will make the geometrical deviation from a sphere larger and the values reported for the earlier fractions less plausible. Nevertheless, it is interesting to compare the zeta potential measured for the raw unsorted EA-SWCNTs used in our previous work[26] (−15.8 mV) to any of the fractions after ATPE/SEC separation. This suggests that the final zeta potential of the SWCNTs is in fact dependent on the processing steps applied.

SWCNT films from each fraction were prepared with the custom-made microfluidic dead-end filtration setup described in detail by Rust et al.[26] and shown schematically in **Figure 2**A.
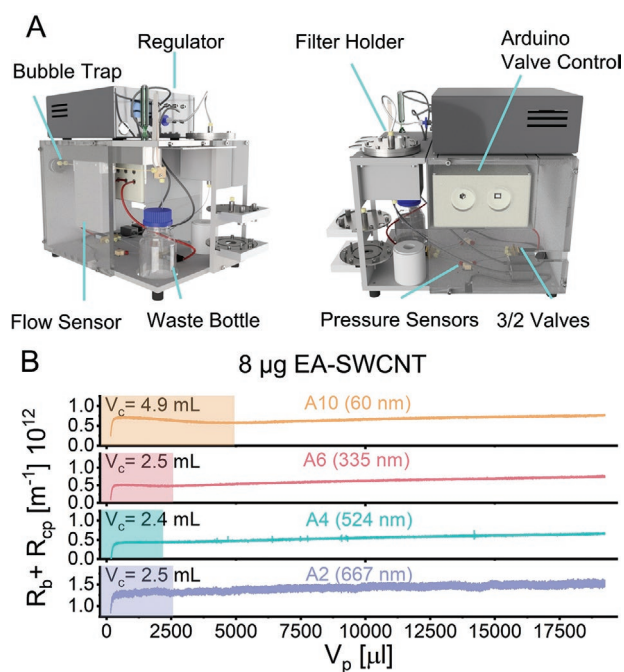

Figure 2. A) Custom microfluidic dead-end filtration setup used for the production of the aligned carbon nanotube thin films. A detailed description of the functionality, capabilities, and calibration protocols can be found here.[26] B) The filtration resistance, which consists of the CP resistance (R_{cp}) and the blocking resistance (R_b), as measured during the slow filtration regime (100 µL min^{-1}) for 8 µg of EA-SWCNT dispersed in 0.02 % DOC and diluted to 20 mL with H$_2$O filtered onto a membrane area A_m= 3.81 cm^2.

Previously, the total mass of SWCNTs filtered was shown to be an important parameter to achieve global alignment and films containing 8, 12, and 24 µg SWCNTs deposited onto a membrane area of A_m= 3.81 cm^2 were made for each length fraction. For each fraction, the highly concentrated stock solution was diluted to an intermediate solution with 8 µg mL^{-1} SWCNTs (0.04 % DOC), and 1, 1.5, or 3 mL of that intermediate solution was diluted once more to a final volume of 20 mL with deionized water, leading to the SWCNT/DOC concentrations found in the Supporting Information (Figure S3, Supporting Information). The filtration consisted of a slow flow (100 µL min^{-1}) step for a majority (19.25 mL) of the volume followed by a fast filtration (500 µL min^{-1}) step during the final 750 µL. These conditions were chosen based on our previous study to globally align unsorted EA-SWCNTs on the same batch of 80 nm pore size membranes. The filtration resistance, which is the sum of the blocking resistance (R_b) (the accumulation of mass on the membrane) and resistance from CP (R_{cp}), was obtained by subtracting the membrane resistance $R_m = 2.43 \times 10^{12}$ m^{-1}[26] from the total resistance (R_{tot}) as shown in Figure 2B for a total filtered SWCNT mass of 8 µg. The filtration resistance curves for 12 and 24 µg can be found in Figure S4, Supporting Information. In our previous work, we stated that the optimum volume rate for the slow filtration step to globally align the CNTs can be identified by minimizing the CP regime. This corresponds to the initial volume during which the carbon nanotubes are floating above the membrane and have not yet caused an increase in the filtration resistance. Once a critical volume (V_c) is reached, cake filtration begins to occur and this manifests itself as a linear increase in resistance; such an effect has also been identified by others to be crucial for SWCNT alignment.[25,26] Despite a variation of both SWCNT mass and length in this study (increases to either are predicted to reduce the size of V_c), no obvious impact on the CP regime could be observed.[26] This observation is potentially due to the use of highly dilute SWCNT solutions, or because the effect is greatest for changes in the volume rate, which in this work was set to 100 µL min^{-1}.

The resulting SWCNT films were imaged by scanning cross-polarized microscopy, with automatic stitching of multiple cross-polarized images (5× magnification) such that the complete 22 mm diameter circle of each SWCNT film is mapped. Bright (SWCNT alignment direction at 45° to the analyzer polarization) and dark (0° or 90° to the analyzer polarization) positions are shown. The alignment vectors were manually identified by rotating the sample and visually maximizing the intensity at the brightest position close to the center for each film, and then rotating the film by 45° from that position for the dark image. If no clear contrast difference could be found (due to a lack of SWCNT alignment), then an arbitrary bright position was chosen and the dark position was defined to be 45° offset from that. One half of the SWCNT film is shown for each orientation in **Figure 3** and full film images can be found in Figure S5, Supporting Information. Additionally, representative 5× magnification images of all films are shown in Figures S6–S8, Supporting Information. A portion of each film was also transferred to a silicon substrate[25] such that the side of the film facing the membrane during filtration could be imaged, Figures S9–S11, Supporting Information.
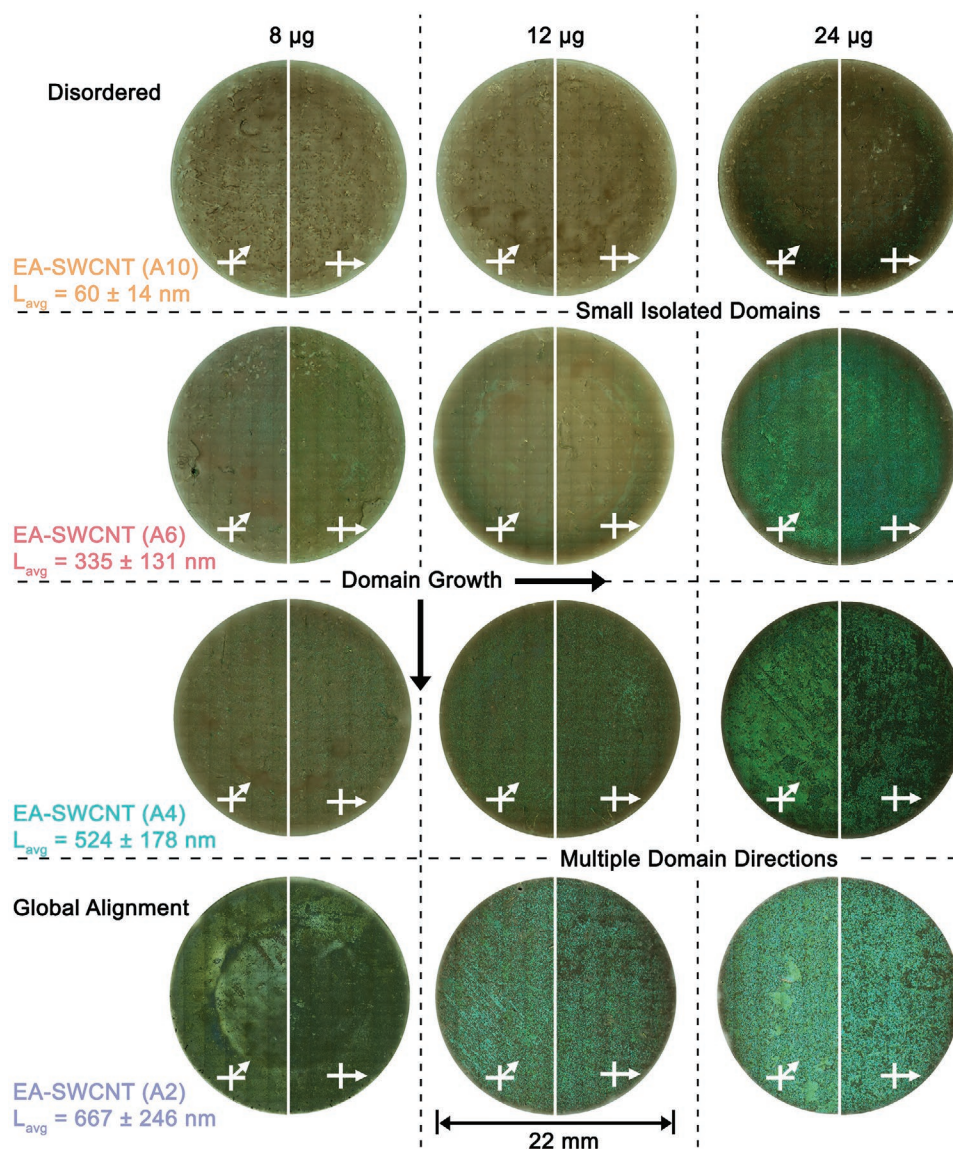
Figure 3. Cross-polarized microscopy of one half of an EA-SWCNT film from the length fractions A10–A2 in the bright (45°) and dark (0°) orientation. Images were recorded with the SWCNT film on the PCTE membrane.

A comparison of both sides of the film (removing the membrane)[25] suggests that the morphology of the SWCNT film is consistent throughout its entire thickness. Machine vision was used to quantify the SWCNT domain size in each of the films.[26] Examples of the detected domains are reported in **Figure 4**A. Depending on the sample, one of two modes of detection was used, if the domain size was significantly smaller than the image size and full-sized domains could be identified in the image, then the domains were measured directly (i.e., 12 µg film of A2, $A_{\text{avg A2 12 µg}} = 2009 \ \mu m^2 \pm 12\ 344 \ \mu m^2$). If the image contained large domains that exceeded the image-area (i.e., 8 µg film of A2) then the software would detect the grain-boundaries and subtract this area from the total image area ($A_{A2\ 8\ µg} = 2.329 \ mm^2$). The cross-polarized images and the detected domains or grain boundaries are shown in Figures S12–S14, Supporting Information. Figure 4B plots the grain size distribution as a histogram

along with the corresponding normal distribution, from which the average domain size and respective standard deviation were calculated in Figure 4C.

For the A10 ($L_{\text{avg}} = 60 \ nm \pm 14 \ nm$) fraction, small isolated SWCNT domains (bright spots in cross-polarized microscopy) can clearly be seen for the 24 µg ($A_{\text{avg A10 24 µg}} = 229 \ \mu m^2 \pm 643 \ \mu m^2$) film, whereas for 8 µg ($A_{\text{avg A10 8 µg}} = 184 \ \mu m^2 \pm 249 \ \mu m^2$) film and 12 µg ($A_{\text{avg A10 12 µg}} = 194 \ \mu m^2 \pm 320 \ \mu m^2$) they were most often much smaller and barely visible. These bright spots correspond to small locally aligned domains of SWCNTs, however, because they can be seen in both the "bright" and "dark" cross-polarized microscopy images, they do not have a common alignment direction. For the A6 ($L_{\text{avg}} = 335 \ nm \pm 131 \ nm$) film, these small SWCNT domains are now visible for all masses and in the case of the 24 µg film, it is particularly evident that the domain size
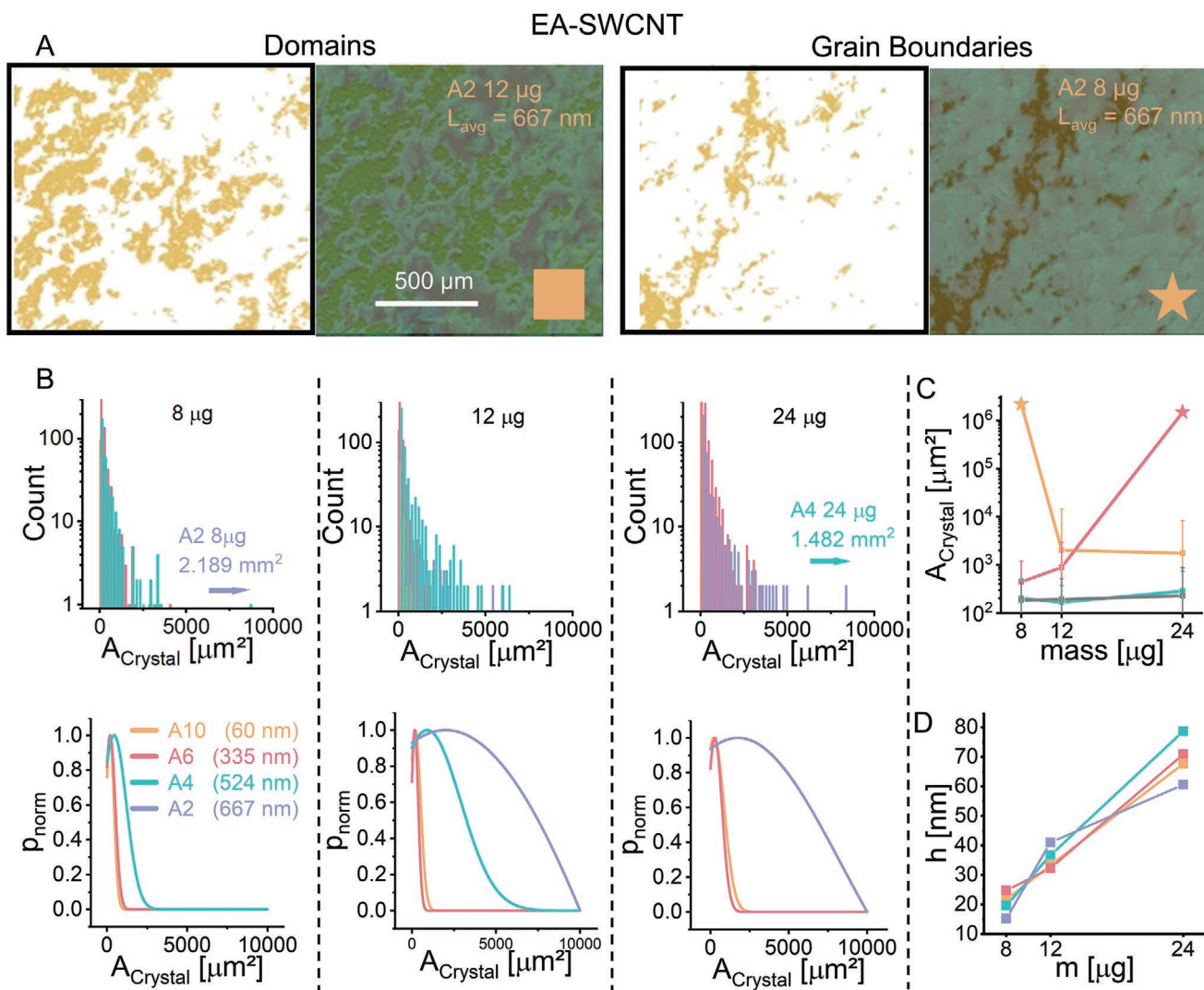
Figure 4. A) The two machine vision techniques used to characterize the domain size. Small domains were measured directly (A2, 12 µg, box) or indirectly by subtracting the grain boundary from the entire pixels in the image (A2, 8 µg, star). (B) Histograms and a normal distribution of the domain-sizes which are summarized in ((C). (D) Film height measured by AFM.

($A_{avg\ A6\ 24\ \mu g} = 284\ \mu m^2 \pm 456\ \mu m^2$) has increased relative to A10. A slight increase in domain size ($A_{avgA6\ 12\ \mu g} = 168\ \mu m^2 \pm 205\ \mu m^2$, $A_{avgA6\ 24\ \mu g} = 284\ \mu m^2 \pm 456\ \mu m^2$) is also observed between the 12 and 24 µg films of A6. The A4 ($L_{avg} = 524\ nm \pm 178\ nm$) film follows the same trend ($A_{avgA4\ 8\ \mu g} = 441\ \mu m^2 \pm 763\ \mu m^2$, $A_{avgA4\ 12\ \mu g} = 904\ \mu m^2 \pm 1992\ \mu m^2$) and has domains that are again larger than A6 but in the case of 24 µg film these become connected and have a common alignment direction. This is evidenced by a clear contrast difference between the bright and dark cross-polarized light images shown in Figure S8, Supporting Information. However, despite the area of the connected domains being large ($A_{avgA4\ 24\ \mu g} = 1.482\ mm^2$), it can be seen in Figure 3 and Figure S5, Supporting Information, that multiple alignment directions still exist across the entire film. Researchers on this topic suspect that there is variation in the quality of membranes with respect to the factors resulting in successful global filtration,[24a,40] for example, manufacturing differences in the density and alignment of

grooves present on the membrane. Global alignment might be possible using this fraction and film mass loading, but we were lacking the sample mass needed to test this hypothesis. Even larger connected areas can be seen for the A2 ($L_{avg} = 667\ nm \pm 246\ nm$) dispersion for the 8 µg film, but in this case, these areas now encompass most of the membrane, and the sample was considered globally aligned. An increase in the deposited mass of A2 led to a more disordered film. While the domain size ($A_{avgA2\ 12\ \mu g} = 2009\ \mu m^2 \pm 12\ 344\ \mu m^2$, $A_{avgA2\ 24\ \mu g} = 1758\ \mu m^2 \pm 456\ \mu m^2$) remained almost constant, and even slightly decreased, we suspect that the amount of domains increased to a point where the combined domain area surpassed the area of the membrane, eventually disturbing the global order. The same phenomenon has been previously reported here,[26] with unsorted EA-SWCNT and increases in mass from 24 µg to 32 µg.[26]

As a next step of characterization, film thicknesses measured using AFM topographies (Figure S15, Supporting Information)

2206774 (6 of 13)

ADVANCED
SCIENCE NEWS
www.advancedsciencenews.com

NANO · MICRO
small
www.small-journal.com

were determined after film transfer to Si wafers and are shown in Figure 4D. The values were evaluated by the step height between the film and substrate, Figure S16, Supporting Information. The smaller length sorted fractions (A10, A6, and A4) show a linear relationship between film height and mass, while A2 appears to become compacted with an increase in mass around 8 µg total deposited mass. In our previous study, we found the films to compact close to the mass needed for global alignment. We suspect that larger masses would be needed for A4 to show the plateau, as a 24 µg film might be sufficient for global alignment.[26] Scanning electron microscopy (SEM) images of the films transferred to Si wafers on small scales (2×2 µm^2) corroborate that A10 and A6 predominately form smaller domains or that they are even completely disordered, Figure S17, Supporting Information. Images taken from films of A4 and A2 are considerably more difficult to interpret. On the length scale measured by an SEM, each of these films appears to be highly aligned. Indeed, this highlights how misleading SEM can be when trying to verify global alignment and we would like to urge the community to rely more heavily on large-area techniques like linear dichroism, cross-polarized microscopy, and S_{2D} evaluation by Raman-mapping in the future.

The importance of SWCNT length to the domain size and consequently the global alignment process motivated us to apply our findings to small-diameter SWCNTs. These SWCNTs are considerably more difficult to deposit in an aligned fashion than the EA-SWCNTs and this is the reason why only a few reports exist on their use. Conventional wisdom suggests that a variation in the initial volume rate, the control mode (constant flux J, constant p_{TMP}, constant pressure p_{in}) fast filtration volume rate, or pore-size of the membrane (50, 80, 100, and 200 nm) will allow them to be aligned and that it is only a matter of process optimization. Indeed, upon comparison of the average length of surfactant dispersed CoMoCAT SWCNTs (L_{avg} = 798 nm ± 545 nm) and their zeta potential ($\zeta_{CoMoCAT}$ = −29.5 mV) to the longest A2 EA-SWCNTs fraction (L_{avg} = 667 nm ± 246 nm, ζ_{A2} = −30 mV), their global alignment appears to be only a matter of optimization. However, in our experiments to optimize the process parameters we were unable to identify a meaningful trend or achieve a reliable improvement in alignment. As an example, Figure S18, Supporting Information, shows cross-polarized microscopy images of CoMoCAT SWCNTs filtered onto an 80 nm pore-sized membrane at varying volume-rates during the slow flow step. It might appear that some of the regions are aligned, and upon closer inspection with an SEM, Figure S19, Supporting Information, aligned domains with sizes up to 10×10 µm^2 can be found. These domains are large enough to provide a high S_{2D} value when measured by single-point Raman spectroscopy, and if these are then imaged by an SEM with the appropriate magnification it is not possible to distinguish them from the globally aligned EA-SWCNTs films shown in Figure S17, Supporting Information. We speculate that this phenomenon could be the source of data in previous reports on small diameter SWCNTs, in which the small spot measured leads the S_{2D} values to significantly exceed values measured by larger area sampling methods; and that global alignment may not have actually been achieved.

Using identical filtration parameters to the EA-SWCNTs (mass diluted to 20 mL with H$_2$O, 100 µL min^{-1} slow filtration, 500 µL min^{-1} fast filtration for the last 750 µL, and 80 nm pore size) SWCNT films from the length sorted CoMoCAT fractions B2 (952 nm ± 431 nm) and B4 (648 nm ± 310 nm) were prepared. Total masses of 8 and 12 µg were used and the concentration of each fraction was again evaluated by the approach outlined here,[26] Figure S3, Supporting Information. Cross-polarized microscopy images of one-half of the SWCNT film are shown in **Figure 5** and full film images can be found in Figures S20 and S21, Supporting Information. Representative 5× magnification images on the membrane and after transfer to a silicon substrate are shown in Figures S22–S24, Supporting Information, and machine vision was again used to evaluate the SWCNT domain size, Figures S25 and S26, Supporting Information. Compared to the non-length sorted CoMoCAT films, Figures S18 & S19, Supporting Information, the domain size of the B4 films was slightly smaller (8 µg: 234 µm^2 ± 383 µm^2, 12 µg: 158 µm^2 ± 195 µm^2) and this is consistent with their shorter length (648 nm ± 310 nm vs 798 nm ± 545 nm). Essentially, B4 behaved like the unsorted fraction and had all its associated problems in achieving global alignment. On the contrary, films made from 8 µg of B2 (L_{avg}= 952 nm ± 431 nm) had significantly larger domain sizes (1467 µm^2 ± 2542 µm^2) and these became even larger (2.329 mm^2) for the 12 µg sample. Once again, the morphology of the film was the same on the front and back of the film, but despite the dramatic improvement in the domain size, the individual domains still did not have a common alignment direction.

In our previous work, we showed that intentional surface texturing of the PCTE membrane by a hot embossing process can improve the alignment of SWCNTs.[26] Here we also hot embossed (HE) a square containing a stripe pattern with line widths of 150, 300, 450, and 600 nm in each of the four quadrants into the membrane, and repeated the filtration of 8 µg of B2 and B4, Figure 5. Although the B4 SWCNTs did not appear to benefit from the template and the film remained disordered, the longer B2 film now showed large range order in the direction of the template, Figure S24, Supporting Information. The domain-size also slightly increased to (2176 ± 5504) µm^2 but showed no correlation to the width of the striped patterns. SEM images can be found in Figure S27, Supporting Information. Considering that the size of the single SWCNT domains on both pristine and hot embossed membranes is similar, we propose that the growth of the domains in highly dilute systems (0.53 µg mL^{-1}) depends on the attractive and repulsive forces between the SWCNTs as well as the SWCNTs and the membrane, and that the alignment director can be given by the grooves of the membrane. This is slightly different from our previous work,[26] in which we filtered much greater SWCNT concentrations (8 µg mL^{-1}) and found that the edge of a groove was a preferential deposition site.

In order to quantify the angular dependence of the absorption, a similar film made with an HE membrane and CoMoCAT (B2) SWCNTs was transferred to an ITO-coated glass substrate and measured in transmittance using a spectrometer and a Glan–Thompson polarizing prism, Figure S28, Supporting Information. The highest and lowest absorption measured with the SWCNTs being parallel and perpendicular
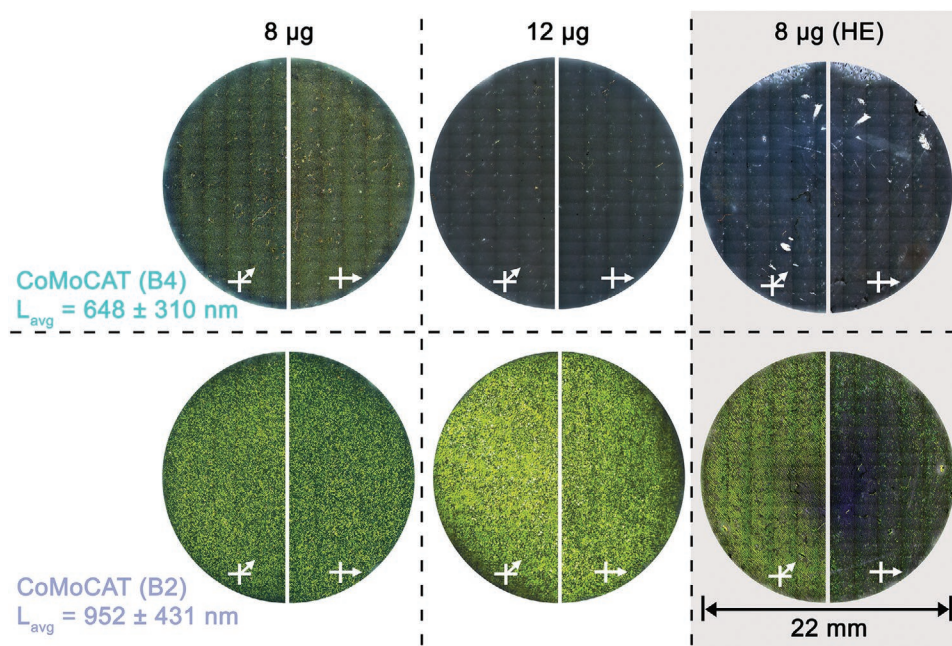
ADVANCED
SCIENCE NEWS
www.advancedsciencenews.com

NANO · MICRO
small
www.small-journal.com

Figure 5. Cross-polarized microscopy of one half of a CoMoCAT film from the length fractions B4 and B2 in the bright (45°) and dark (0°) orientation and on pristine and hot-embossed (HE) membranes.

to the incident light source were determined to be at 5° and 95°, respectively and were thus used to determine the dichroic ratio $\Delta(\lambda)$, **Figure 6**. Using the dichroic ratio at the wavelength of the Raman laser for the SWCNTs used ($\Delta_{CoMoCAT}$ (532 nm) = 1.58 and $\Delta_{EA-SWCNT}$ (532 nm) = 1.55),[26] allows for a map of the order parameter S_{2D} via Raman spectroscopy following the approach of Zamora-Ledezma et al.[12c] over 625 μm^2, yielding $S_{2D\ max} \approx 0.76$ for the EA-SWCNT (A2) and ≈ 0.6 for the CoMoCAT (B2) films. The measured intensities of the different optical configurations (I_{HH}, I_{HV}, I_{VV} and I_{VH}) are shown in Figure S29, Supporting Information. Compared to the values obtained for our previous global aligned film using EA-SWCNT and similar filtration parameters ($S_{2D\ max} \approx 0.83$),[26] the films shown here are slightly less aligned. For CoMoCAT SWCNTs with comparable length, He et al. stated a spot measurement with $S_{3D} \approx 0.73$,[13] which cannot be compared to S_{2D} directly.

In the past, it has been suggested to describe the formation of domains with the classical Onsager argument involving a crystal phase formation which is valid for high concentrations of rigid rods.[41] By estimating the typical SWCNT density of an enriched phase to be 1.5 g mL^{-1},[42] Lagerwall et al. suggested that a ratio of $\frac{d_t}{L} = 10^{-3}$ should facilitate the formation of a nematic phase and thus the formation of domains.[43] The concentrations of the SWCNT dispersions used in this study ranged from 0.53 μg mL^{-1} to 1.6 μg mL^{-1}. In the bulk, this is six orders of magnitude lower compared to different from the concentration used by Lagerwall et al., but the actual concentration in the enriched 2D plane is unknown but certainly significantly higher than the bulk. According to Onsager's model, a lower ratio has a higher tendency to grow crystals and this would predict that in-fact only the unsorted and B2 CoMoCAT sample would be able to form and grow domains, Figure S30, Supporting

Information. However, this clearly contradicts our observation and that of others.[13,25,26] This is likely due to the membrane not being represented, which provides a driving force for alignment by morphology, that is, grooves,[24a] directional charges,[13,25] or a directional flow patterns,[26] nor the sharp change in hydrodynamics and concentration near the surface. In either case, however, the SWCNTs must be reorienting as they approach the surface for any aligned film. One manner to explore the ordering of the CNTs parallel to the membrane surface is to analyze the total potential (Φ_{TOT}) according to Wu et al.,[35] which describes the SWCNTs as stiff rods, which might not be true for small diameter SWCNTs when they get longer, but should not change the area interacting with the membrane significantly.[44]

The total potential is the sum of the repulsive electric double layer and attractive van der Waals forces between the membrane and SWCNTs. In the case that the sum of these interactions are positive, the SWCNTs are kept "afloat" and enriched in a 2D plane of minimum potential above the membrane during the initial stages of filtration. This phenomenon is described by CP, which also stems from a concentration gradient that establishes above the membrane during filtration,[45] but both forces depend on the length and diameter of the SWCNT. Akin to our previous study,[26] we utilized the DLVO formulas derived by Wu et al.[35] to describe the superposition of the electric double layer potential (Φ_{EDL}) and van der Waals potential (Φ_{VW}) acting on an individual SWCNT parallel to an 80 nm pore-size membrane surface. The resulting total potential (Φ_{TOT}) depends on the distance to the surface, z, and has a primary minimum close to the surface, followed by a potential barrier and a secondary minimum. In order to perform these calculations, knowledge of the ionic strength at the membrane surface is required. A DOC concentration of 0.04 wt.% in the bulk corresponds to an ionic strength of 1 mmolL^{-1}, which is
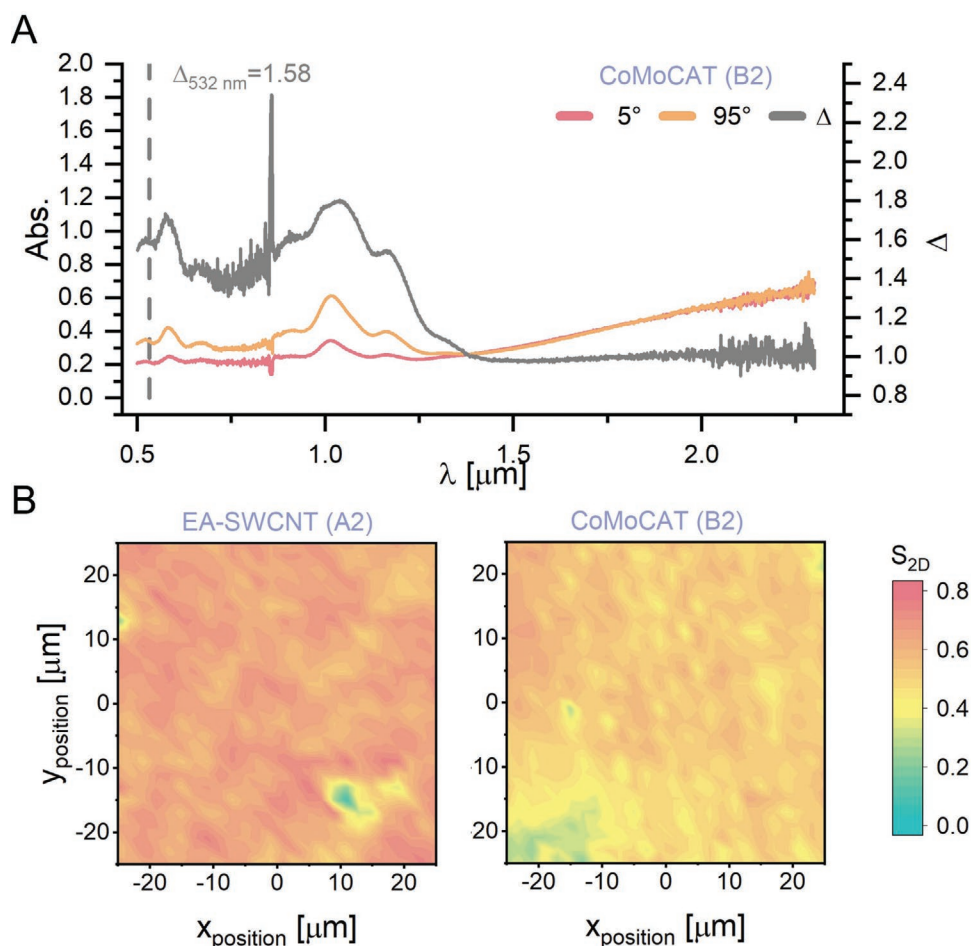
Figure 6. A) Dichroic ratio of a globally aligned CoMoCAT (B2) film made with an HE membrane and transferred to an ITO glass substrate. B) For the calculation of the S_{2D} maps, dichroic ratios of $\Delta_{EA-SWCNT} = 1.55$[26] and $\Delta_{CoMoCAT} = 1.58$ for a laser excitation at 532 nm were used. The $S_{2D\ max}$ values reach ≈ 0.76 for the EA-SWCNT (A2) and ≈ 0.6 for the CoMoCAT (B2) films.

unlikely to increase at the membrane, as the molecule (MW 0.414 kDa) is not large enough to get retained. For this reason, an ionic strength of 1 mmolL^{-1} is chosen for the curves shown in **Figure 7**A. For the case, that the DOC concentration might increase at the membrane, due to absorption or retention of the micelles formed, calculations for 1, 10, and 100 mmolL^{-1} can be found in Figure S31, Supporting Information. However, the impact on the length needed for a CoMoCAT SWCNT is limited to around 50 nm. More details on the calculation can be found in the Supporting Information.

In Figure 7A, Φ_{TOT} is plotted for all fractions and diameters used in this work up to a distance of $z = 40$ nm from the membrane. The secondary minimum located at $z \approx 27$ nm is too small compared to the primary energy barrier to the surface ($\Phi_{TOT\ max} \approx 25$ to 150 kT, in which k is the Boltzmann constant and T the temperature) to be visible in Figure 7A and an enlarged view is shown Figure 7B for every SWCNT, respectively. By comparing the depth of secondary minima with the experimental results shown above it can be concluded that fractions with a secondary minimum equal to- or deeper than -0.075 kT form domains and that these increase in size with increasing SWCNT mass. This threshold value changes with

the ionic strength used and for reference, an ionic strength of 100 or 1 mmolL^{-1} corresponds to a secondary minimum with a depth of -1.102 and -0.058 kT, respectively. For the large diameter EA-SWCNTs ($d_t \approx 1.4$ nm) this was true for the fractions A4 ($L_{avg} = 524$ nm ± 178 nm) and A2 ($L_{avg} = 667$ nm ± 246 nm), while only the longest small diameter CoMoCAT SWCNTs (B2) ($d_t \approx 0.78$ nm, $L_{avg} = 952$ nm ± 431 nm) showed the capacity to grow domains with increasing mass. On the contrary, when the secondary minimum is shallower than the threshold value, the domains stagnate and do not increase in size with increasing mass, as it could be observed for all other fractions. However, it is important to acknowledge that all three threshold values are small relative to the thermal energy available at room temperature as DLVO calculations do not account for the volumetric flow rate used during filtration, or the interaction between neighboring carbon nanotubes during enrichment. Nevertheless, a connection between global alignment and a small secondary minimum could explain the importance of finding the exact volume rate during the slow-filtration regime at the beginning of the filtration.[13,25,26]

Under the assumption that a secondary minimum with a depth of at least -0.058 kT is required, the smallest required
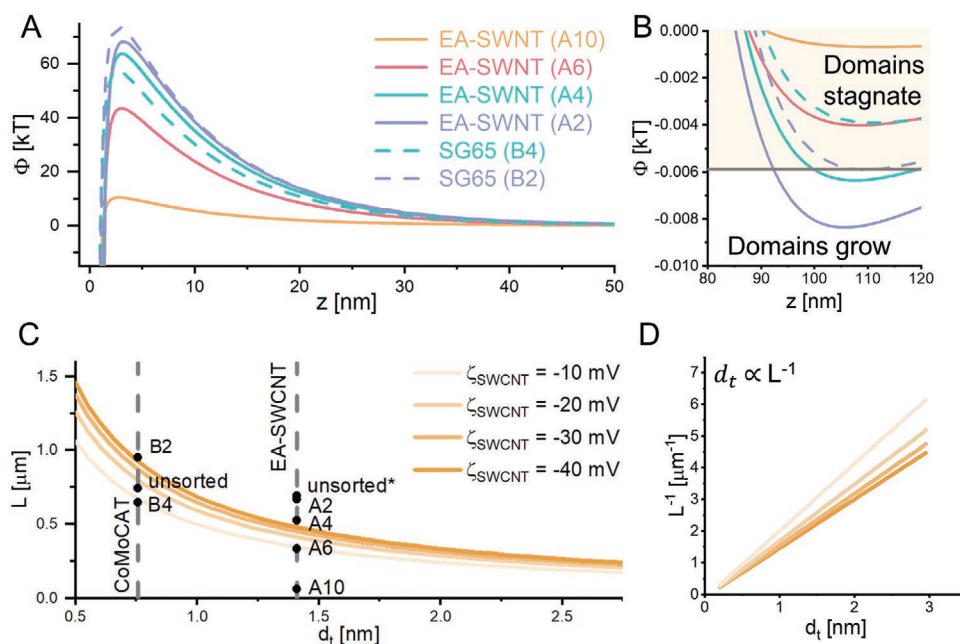
ADVANCED
SCIENCE NEWS
www.advancedsciencenews.com

NANO · MICRO
small
www.small-journal.com

Figure 7. A) DLVO calculations for all SWCNT fractions used in this publication, showing the Φ_{TOT} to a distance, $z = 50$ nm from the membrane surface. B) An enlarged view of the secondary minimum of Φ_{TOT} at $z \approx 28$ nm. C) All combinations of length L, diameter d_t, and zeta potential of the SWCNT ζ_{SWCNT} with a sufficient depth of the potential secondary minima for global alignment. D) The curves shown in ((C) follow a $d \propto L^{-1}$ relationship .

length (L) of a hypothetical SWCNT with a given diameter (d_t) and zeta potential ζ_{SWCNT} is shown in Figure 7C. The zeta potential was varied between –10 and –40 mV with the hope that the zeta potential measured by other researchers for their SWCNTs will most likely fall within this range. Figure 7C can be understood as follows: A SWCNT will form domains of sufficient size for global alignment only if it is long enough, and this is the case when it coincides with or is above the respective boundary curve for a given zeta potential. Every combination of d_t and L below the boundary curve does not have a sufficient secondary minimum for domain growth. This rule can be further corroborated by including all fractions and unsorted carbon nanotubes used in this and the previous publication[26] (marked with a star). It can now also be seen why small diameter SWCNTs are more difficult to align: The influence of the ζ_{SWCNT} decreases with the length of the SWCNTs and this makes precise control over their length less important. For reference, a SWCNT dispersion prepared by sonication, which is the most common method, usually has a number average length of less (or much less) than 600–800 nm and very rarely > 1000 nm. For EA-SWCNTs this does not pose a problem, but for the small diameter SWCNTs their length is simply too short, or the required zeta potential unattainable, for global alignment. Importantly, as seen in Figure S29, Supporting Information, the relationship between the required length for alignment and the SWCNT's diameter was not found to vary significantly for the ionic strengths considered in this work. It is worth mentioning that He et al., have claimed global alignment of CoMoCAT raw material with $L = 420$ nm[13] and Katsutani et al. with $L = 200$ nm.[29a] In the filtration regime explored in this effort, such films would only form small aligned domains with limited registration to each other, not achieving universal and strong global alignment along the same vector. Plotting the

curves in Figure 7C with respect to an inverse length L^{-1}, yields an inverse proportional relationship $d_t \propto L^{-1}$, Figure 7D, which allows for a linear fit $L^{-1} = m_{\zeta SWCNT} d_t + b_{\zeta SWCNT}$, with $m_{\zeta SWCNT}$ and $b_{\zeta SWCNT}$ being the slope and intercept. The fitting parameters of the corresponding curves can be found in the Supporting Information and are more accurate for higher charged SWCNTs, due to the curves being slightly more linear.

3. Conclusion

Utilizing length-sorted SWCNT fractions with average diameters of ≈ 1.4 (EA-SWCNT) and ≈ 0.78 nm (CoMoCAT SWCNTs), we investigated the necessary length and mass at a given zeta potential to achieve spontaneous global alignment with the dead-end filtration method. We showed that the best alignment for EA-SWCNT ($S_{2D} = 0.76$) and CoMoCAT-SWCNT ($S_{2D} = 0.66$) was achieved with an effective SWCNT concentration of 0.53 μg mL^{-1} in the bulk solution and for the longest SWCNT fractions. Long fractions of EA-SWCNTs (A4) and (A2) were found to increase their domain size significantly with mass but the smaller fractions (A6) and (A10) appeared to stagnate and remain small. For CoMoCAT, only the longest fraction (B2), was able to grow domains with increased film mass but still required a template to align them in a common direction. Here, interestingly the size of the domains remained constant and only their directionality was influenced by the pattern. Upon comparison of our experimental results to DLVO calculations we also suggest that there exists a threshold value for the secondary minimum for a given combination of diameter d_t, length L, ionic strength I, and a given zeta-potential of the SWCNTs ζ_{SWCNT} in order for global alignment to occur. Following this boundary condition, we derived a relationship

between diameter and length that follows the proportionality $d_t \propto L^{-1}$. We hope that this relationship can be used as a guide for future experimentalists to find the required length or zeta potential to globally align chirality-sorted SWCNTs, which are expected to open-up a wide range of new applications. Nevertheless much more work is still required to understand the importance of the homogeneity in length (low standard deviation) of the material used and other forces acting on the SWCNTs including Brownian forces, viscous drag forces, buoyant forces, and gravitational forces.[46]

4. Experimental Section

Certain equipment, instruments, or materials were identified in this paper in order to adequately specify the experimental details. Such identification does not imply recommendation by the National Institute of Standards and Technology (NIST) nor does it imply the materials were necessarily the best available for the purpose. Except where specified otherwise, uncertainty in this contribution was reported as one standard deviation.

Length Sorting of SWCNTs: Length separation of the SWCNT dispersions was performed via size-exclusion chromatography (SEC) in the manner described by Khripin et al.[38] The SEC separation was conducted over three SEC columns (Sepax Technologies) packed with 5 µm silica beads with nominal pore sizes of 200, 100, and 30 nm, using a GE ÄTKA Purifier HPLC system. SWCNTs were injected and eluted with 10 g L^{-1} DOC pumped at a flowrate of 5 mL min^{-1}; 5 mL fractions were collected.

Filtration of Films: All concentrated dispersions were diluted with deionized water (18.2 MΩcm, pH = 6.93) from an Arium pro UV (Sartorius), to reach the required mass (8 µg, 12 µg or 24 µg) in a 20 mL volume. This corresponds to the maximum volume of the filtration setup. A detailed description of the microfluidic setup, its calibration, and installation of membranes can be found here.[26] If not described otherwise, all films were filtered with an initial volume-rate of 100 µL min^{-1} (J = 0.26 mm min^{-1}) until only 750 µL of dispersion remained. This was then pushed down with a fast filtration volume rate of 500 µL min^{-1} (J = 1.31 mm min^{-1}) and additional nitrogen was supplied until the film was dry. All membranes (47 mm diameter, 80 nm pore size, pore density of 6×10^8 cm^{-2}, thickness of 25 µm) were obtained from it4ip.

Film Transfer: SWCNT films were transferred to Si-wafers (CrysTec, polished and etched, thickness 525 µm, p-type, specific resistance > 1 Ωcm) using the method outlined by Walker et al.[25] Membranes were dissolved with Chloroform (99.2 % stabilized with 0.6 % ethanol, VWR chemicals) and adhered to the surface at 50 °C.

Spectroscopy: UV–vis–NIR absorbance spectra of nanotube dispersions for concentration determination were collected on a Cary 500 spectrometer in the wavelength range 1880 to 200 nm in 1 nm increments through a 1 mm glass cuvette, while the measurement identifying the peaks was carried out on a Cary 5000 spectrometer in the same wavelength range/increments using a 1 mm quartz cuvette. A Lambda 1050 spectrometer (Perkin Elmer) with an integrating sphere module, 2 mm beam spot, and Glan–Thompson polarizing prism was used to determine the dichroic ratio. Polarized Raman scattering maps (Horiba LabRAM HR Evolution) were collected with ≈1 mW of 532 nm laser excitation over a spectral range of 1500 to 1650 cm^{-1}. Pump and collection polarization control was achieved via stage and analyzer rotation, respectively, referencing a stage position that yielded the highest integrated intensity of the high-energy G$^+$ vibrational mode (≈ 1590 ± 3) cm^{-1} as the VV configuration. Points were taken every 2 µm over a 50 × 50 µm area, with 2 accumulations of 1.5 s each for de-spiking and improved signal-to-noise ratio.

Scanning Electron Microscopy: All images were taken, using a Zeiss Ultra Plus with a 30 µm aperture and an acceleration voltage of 2 kV.

Cross-Polarized Light Microscopy: A Leica DM6 M light microscope was used to capture cross-polarized measurements of the membrane and transferred films. The images were obtained in reflectance with two linear polarizers, whereby the incident light was polarized by 90° with respect to the analyzer. To record the images for dark (0°) and bright position (45°), a rotational stage was placed on the microscope table and rotated to identify the position with maximum intensity. For the large area scans of the film on the membrane, several 5 × magnified images were stitched together automatically, using the software provided by Leica. All images were recorded with the same brightness and exposure time. Images were analyzed with ImageJ and the open-source extension shape logic detecting the individual grains, with two iterations performed, a minimal pixel threshold of 50 and a maximal pixel threshold comprising all pixels of the image.

AFM Microscopy: Topographies were recorded with a Dimension Icon, Bruker with NSC 19 cantilevers (µmasch) with a resonance frequency of 65 kHz and a force constant of 0.5 Nm^{-1}. Imaging was performed in standard tapping mode in air and a resolution of 1024 lines. All topographies were first order flattened and evaluated using open-source Gwyddion. For the length determination, 30 µL of ten times diluted dispersion were spin-coated onto a silicon wafer at 2000 rpm for 3 min.

AUC Length Determination: AUC was conducted in a Beckman-Coulter XL-I analytical ultracentrifuge with an AnTi-50 rotor and standard 12 mm optical pathlength epon-charcoal cells with sapphire windows. Measurements were performed at a rotation rate of 2932 rad s^{-1} (28 kRPM) on highly diluted samples to avoid significant deviation from ideal sedimentation readily observed for extended colloids. The temperature was 20.0 °C and ensured by a minimum of 1.5 h of temperature equilibration. The density and viscosity of the exact 10.0 g L^{-1} DOC solutions at 20.0 °C were measured using an Anton-Parr DMA 5000 M–LOVIS 2000 ME densitometer-viscometer. Analysis of the recorded radial absorbance profiles as a function of time was conducted using the numerical fitting software SEDFIT V15.01b and V16.1c.[47] Sedimentation was modeled using the c(s) model as length-sorted SWCNT fractions exhibit narrow friction factor distributions, negating the need for c(s,f/f$_0$) modeling. The meniscus and noise were fit for each experiment and agreed well with the apparent positions in the data. Conversion of measured sedimentation coefficient distributions to length distributions was conducted by using the hydrodynamic models for cylinders[48] and known geometric and measured solution and SWCNT parameters.[49]

Zeta Potential of SWCNT Dispersions: The zeta potential of the dispersions was measured with a Zetasizer Nano ZS, Malvern. The standard Smoluchowski model was used to evaluate the zeta potential from the hydrodynamic radius calculated from the autocorrelation function and the electrophoretic mobility using the integrated PALS system. The solution parameters were selected to be identical to the constants of pure water at 25 °C (v = 0.8872 mm^{2}s^{-1}, n = 1.33, and ε_r = 78.5).

Hot-Embossing: For hot-embossing of the membranes, the shim introduced previously[26] featuring stripes with widths of 150, 300, 450, and 600 nm was used. Structures were imprinted with 16 kN of force and at 120 °C, which is slightly below the glass transition temperature of polycarbonate (147 °C).[24a]

DLVO Calculation: DLVO analysis was realized with the Anaconda 3 jupyter notebook using python 3 with various numpy and scipy packages. The original derivation was described by Wu et al.[40] The used parameters are detailed in the Supporting Information.

Statistical Analysis: For the length analysis using an AFM the following amount of carbon nanotubes were counted: EA SWCNT: n = 58 (A10), n = 133 (A6), n = 190 (A4), n = 382 (A2); CoMoCAT SWCNT: n = 662 (unsorted), n = 232 (B4), n = 111 (B2). For the evaluation of the grain sizes, the following amounts of total domains were counted: EA SWCNT: $n_{8\ \mu g}$ = 120, $n_{12\ \mu g}$ = 81, $n_{24\ \mu g}$ = 511 (A10), $n_{8\ \mu g}$ = 1065, $n_{12\ \mu g}$ = 824, $n_{24\ \mu g}$ = 1560 (A6), $n_{8\ \mu g}$ = 328, $n_{12\ \mu g}$ = 520 $n_{24\ \mu g}$ = 766 (A4), $n_{8\ \mu g}$ = 1, $n_{12\ \mu g}$ = 255, $n_{12\ \mu g}$ = 427 (A2); CoMoCAT SWCNT: $n_{8\ \mu g}$ = 1156, $n_{12\ \mu g}$ = 1851 (B4), $n_{8\ \mu g}$ = 242, $n_{12\ \mu g}$ = 1 (B2). All data is represented as mean ± SD and the curve fits have been done with normalized Gaussian fits. Evaluation of the data has been done with origin pro 2018b.

Supporting Information

Acknowledgements

Conflict of Interest

The authors declare no conflict of interest.

Data Availability Statement

The data that support the findings of this study are available from the corresponding author upon reasonable request.

Keywords

[1] a) M. S. Dresselhaus, G. Dresselhaus, P. Avouris, *Carbon Nanotubes: Synthesis, Structure, Properties and Applications*, Springer, Berlin **2001**; b) A. Jorio, G. Dresselhaus, M. S. Dresselhaus, *Carbon Nanotubes: Advanced Topics in the Synthesis, Structure, Properties and Applications*, Springer, Berlin **2008**; c) R. Saito, G. Dresselhaus, M. S. Dresselhaus, *Physical Properties of Carbon Nanotubes*, Imperial College, London **1998**; d) M. Pfohl, D. D. Tune, A. Graf, J. Zaumseil, R. Krupke, B. S. Flavel, *ACS Omega* **2017**, *2*, 1163.

[2] a) M. Pfohl, K. Glaser, J. Ludwig, D. D. Tune, S. Dehm, C. Kayser, A. Colsmann, R. Krupke, B. S. Flavel, *Adv. Energy Mater.* **2016**, *6*, 1501345; b) M. Pfohl, K. Glaser, A. Graf, A. Mertens, D. D. Tune, T. Puerckhauer, A. Alam, L. Wei, Y. Chen, J. Zaumseil, A. Colsmann, R. Krupke, B. S. Flavel, *Adv. Energy Mater.* **2016**, *6*, 1600890; c) B. J. Landi, M. J. Ganter, C. D. Cress, R. A. DiLeo, R. P. Raffaelle, *Energy Environ. Sci.* **2009**, *2*, 638; d) A. Varga, M. Pfohl, N. A. Brunelli, M. Schreier, K. P. Giapis, S. M. Haile, *Phys. Chem. Chem. Phys.* **2013**, *15*, 15470; e) D. D. Tune, B. S. Flavel, *Adv. Energy Mater.* **2018**, *8*, 1703241; f) L. Wieland, H. Li, C. Rust, J. H. Chen, B. S. Flavel, *Adv. Energy Mater.* **2021**, *11*, 2002880; g) J. L. Blackburn,

ACS Energy Lett. **2017**, *2*, 1598; h) M. S. Arnold, J. L. Blackburn, J. J. Crochet, S. K. Doorn, J. G. Duque, A. Mohite, H. Telg, *Phys. Chem. Chem. Phys.* **2013**, *15*, 14896; i) A. Classen, L. Einsiedler, T. Heumueller, A. Graf, M. Brohmann, F. Berger, S. Kahmann, M. Richter, G. J. Matt, K. Forberich, J. Zaumseil, C. J. Brabec, *Adv. Energy Mater.* **2018**, *8*, 1801913; j) M. Gong, T. A. Shastry, Q. Cui, R. R. Kohlmeyer, K. A. Luck, A. Rowberg, T. J. Marks, M. F. Durstock, H. Zhao, M. C. Hersam, S. Ren, *ACS Appl. Mater. Interfaces* **2015**, *7*, 7428; k) D. D. Tune, N. Mallik, H. Fornasier, B. S. Flavel, *Adv. Energy Mater.* **2020**, *10*, 1903261.

[3] a) P. Avouris, M. Freitag, V. Perebeinos, *Nat. Photonics* **2008**, *2*, 341; b) F. Pyatkov, V. Fütterling, S. Khasminskaya, B. S. Flavel, F. Hennrich, M. M. Kappes, R. Krupke, W. H. P. Pernice, *Nat. Photonics* **2016**, *10*, 420; c) M. Engel, K. E. Moore, A. Alam, S. Dehm, R. Krupke, B. S. Flavel, *ACS Nano* **2014**, *8*, 9324.

[4] a) B. S. Flavel, J. Yu, J. G. Shapter, J. S. Quinton, *J. Mater. Chem.* **2007**, *17*, 4757; b) M. Steiner, M. Engel, Y.-M. Lin, Y. Wu, K. Jenkins, D. B. Farmer, J. J. Humes, N. L. Yoder, J.-W. T. Seo, A. A. Green, M. C. Hersam, R. Krupke, P. Avouris, *Appl. Phys. Lett.* **2012**, *101*, 053123.

[5] a) X. Yu, B. Munge, V. Patel, G. Jensen, A. Bhirde, J. D. Gong, S. N. Kim, J. Gillespie, J. S. Gutkind, F. Papadimitrakopoulos, J. F. Rusling, *J. Am. Chem. Soc.* **2006**, *128*, 11199; b) M. Pfohl, K. Glaser, J. Ludwig, D. D. Tune, S. Dehm, C. Kayser, A. Colsmann, R. Krupke, B. S. Flavel, *Adv. Energy Mater.* **2016**, *6*, 1501345; c) D. D. Tune, F. Hennrich, S. Dehm, M. F. G. Klein, K. Glaser, A. Colsmann, J. G. Shapter, U. Lemmer, M. M. Kappes, R. Krupke, B. S. Flavel, *Adv. Energy Mater.* **2013**, *3*, 1091; d) D. J. Bindl, N. S. Safron, M. S. Arnold, *ACS Nano* **2010**, *4*, 5657.

[6] a) D. D. Tune, B. W. Stolz, M. Pfohl, B. S. Flavel, *Nanoscale* **2016**, *8*, 3232; b) D. Wang, P. C. Song, C. H. Liu, W. Wu, S. S. Fan, *Nanotechnology* **2008**, *19*, 075609.

[7] a) S. J. Kang, C. Kocabas, T. Ozel, M. Shim, N. Pimparkar, M. A. Alam, S. V. Rotkin, J. A. Rogers, *Nat. Nanotechnol.* **2007**, *2*, 230; b) A. Ismach, D. Kantorovich, E. Joselevich, *J. Am. Chem. Soc.* **2005**, *127*, 11554.

[8] a) G. Giancane, A. Ruland, V. Sgobba, D. Manno, A. Serra, G. M. Farinola, O. H. Omar, D. M. Guldi, L. Valli, *Adv. Funct. Mater.* **2010**, *20*, 2481; b) Q. Cao, S. J. Han, G. S. Tulevski, Y. Zhu, D. D. Lu, W. Haensch, *Nat. Nanotechnol.* **2013**, *8*, 180.

[9] a) H. Li, T. C. Hain, A. Muzha, F. Schoppler, T. Hertel, *ACS Nano* **2014**, *8*, 6417; b) M. Engel, J. P. Small, M. Steiner, M. Freitag, A. A. Green, M. C. Hersam, P. Avouris, *ACS Nano* **2008**, *2*, 2445; c) G. J. Brady, Y. Joo, S. S. Roy, P. Gopalan, M. S. Arnold, *Appl. Phys. Lett.* **2014**, *8*, 11614; d) Y. Joo, G. J. Brady, C. Kanimozhi, J. Ko, M. J. Shea, M. T. Strand, M. S. Arnold, P. Gopalan, *ACS Appl. Mater. Interfaces* **2017**, *9*, 28859.

[10] a) M. D. Lynch, D. L. Patrick, *Nano Lett.* **2002**, *2*, 1197; b) R. Krupke, F. Hennrich, H. von Lohneysen, M. M. Kappes, *Science* **2003**, *301*, 344.

[11] L. Jin, C. Bower, O. Zhou, *Appl. Phys. Lett.* **1998**, *73*, 1197.

[12] a) X. Li, Y. Jung, K. Sakimoto, T.-H. Goh, M. A. Reed, A. D. Taylor, *Energy Environ. Sci.* **2013**, *6*, 879; b) E. K. Hobbie, D. J. Fry, *Phys. Rev. Lett.* **2006**, *97*, 036101; c) C. Zamora-Ledezma, C. Blanc, M. Maugey, C. Zakri, P. Poulin, E. Anglaret, *Nano Lett.* **2008**, *8*, 4103; d) D. D. Tune, A. J. Blanch, C. J. Shearer, K. E. Moore, M. Pfohl, J. G. Shapter, B. S. Flavel, *ACS Appl. Mater. Interfaces* **2015**, *7*, 25857; e) P. Kim, S. Baik, K. Y. Suh, *Small* **2008**, *4*, 92; f) J. Q. Li, Q. Zhang, Y. H. Yan, S. Li, L. Q. Chen, *IEEE Trans. Nanotechnol.* **2007**, *6*, 481; g) K. R. Jinkins, J. Chan, R. M. Jacobberger, A. Berson, M. S. Arnold, *Adv. Electron. Mater.* **2019**, *5*, 93117.

[13] X. W. He, W. L. Gao, L. J. Xie, B. Li, Q. Zhang, S. D. Lei, J. M. Robinson, E. H. Haroz, S. K. Doorn, W. P. Wang, R. Vajtai, P. M. Ajayan, W. W. Adams, R. H. Hauge, J. Kono, *Nat. Nanotechnol.* **2016**, *11*, 633.

ADVANCED
SCIENCE NEWS
www.advancedsciencenews.com

NANO · MICRO
small
www.small-journal.com

[14] M. S. P. Shaffer, X. Fan, A. H. Windle, *Carbon* **1998**, *36*, 1603.

[15] B. Dan, A. W. K. Ma, E. H. Haroz, J. Kono, M. Pasquali, *Ind. Eng. Chem. Res.* **2012**, *51*, 10232.

[16] B. King, B. Panchapakesan, *Nanotechnology* **2014**, *25*, 175201.

[17] a) X. Tu, A. R. Hight Walker, C. Y. Khripin, M. Zheng, *J. Am. Chem. Soc.* **2011**, *133*, 12998; b) F. Yang, M. Wang, D. Q. Zhang, J. Yang, M. Zheng, Y. Li, *Chem. Rev.* **2020**, *120*, 2693; c) D. Janas, *Mater. Chem. Front.* **2018**, *2*, 36.

[18] M. S. Arnold, S. I. Stupp, M. C. Hersam, *Nano Lett.* **2005**, *5*, 713.

[19] X. Huang, R. S. McLean, M. Zheng, *Anal. Chem.* **2005**, *77*, 6225.

[20] a) K. E. Moore, M. Pfohl, F. Hennrich, V. S. K. Chakradhanula, C. Kuebel, M. M. Kappes, J. G. Shapter, R. Krupke, B. S. Flavel, *ACS Nano* **2014**, *8*, 6756; b) H. Li, G. Gordeev, S. Wasserroth, V. S. K. Chakravadhanula, S. K. C. Neelakandhan, F. Hennrich, A. Jorio, S. Reich, R. Krupke, B. S. Flavel, *Nat. Nanotechnol.* **2017**, *12*, 1176.

[21] a) M. S. Arnold, A. A. Green, J. F. Hulvat, S. I. Stupp, M. C. Hersam, *Nat. Nanotechnol.* **2006**, *1*, 60; b) H. Gui, J. K. Streit, J. A. Fagan, A. R. H. Walker, C. W. Zhou, M. Zheng, *Nano Lett.* **2015**, *15*, 1642; c) C. Y. Khripin, J. A. Fagan, M. Zheng, *J. Am. Chem. Soc.* **2013**, *135*, 6822.

[22] a) M. Zheng, A. Jagota, M. S. Strano, A. P. Santos, P. Barone, S. G. Chou, B. A. Diner, M. S. Dresselhaus, R. S. Mclean, G. B. Onoa, *Science* **2003**, *302*, 1545; b) D. Yang, L. Li, X. Wei, Y. Wang, W. Zhou, H. Kataura, S. Xie, H. Liu, *Sci. Adv.* **2021**, *7*, eabe0084; c) H. P. Liu, D. Nishide, T. Tanaka, H. Kataura, *Nat. Commun.* **2011**, *2*, 309; d) H. Li, G. Gordeev, O. Garrity, S. Reich, B. S. Flavel, *ACS Nano* **2019**, *13*, 2567.

[23] a) X. Wei, T. Tanaka, T. Hirakawa, Y. Yomogida, H. Kataura, *J. Am. Chem. Soc.* **2017**, *139*, 16068; b) H. Li, G. Gordeev, O. Garrity, N. A. Peyyety, P. B. Selvasundaram, S. Dehm, R. Krupke, S. Cambre, W. Wenseleers, S. Reich, M. Zheng, J. A. Fagan, B. S. Flavel, *ACS Nano* **2020**, *14*, 948.

[24] a) N. Komatsu, M. Nakamura, S. Ghosh, D. Kim, H. Chen, A. Katagiri, Y. Yomogida, W. Gao, K. Yanagi, J. Kono, *Nano Lett.* **2020**, *20*, 2332; b) W. Gao, J. Kono, *R. Soc. Open Sci.* **2019**, *6*, 181605; c) R. Wang, J. Chen, L. Chen, Z. Ye, C. Wu, W. Gao, L. Xie, Y. Ying, *Desalination* **2020**, *494*, 114671; d) P.-H. Ho, D. B. Farmer, G. S. Tulevski, S.-J. Han, D. M. Bishop, L. M. Gignac, J. Bucchignano, P. Avouris, A. L. Falk, *Proc. Natl. Acad. Sci. USA* **2018**, *115*, 12662.

[25] J. S. Walker, J. A. Fagan, A. J. Biacchi, V. A. Kuehl, T. A. Searles, A. R. Hight Walker, W. D. Rice, *Nano Lett.* **2019**, *19*, 7256.

[26] C. Rust, H. Li, G. Gordeev, M. Spari, M. Guttmann, Q. Jin, S. Reich, B. S. Flavel, *Adv. Funct. Mater.* **2022**, *32*, 2107411.

[27] J. S. Walker, Z. J. Macdermid, J. A. Fagan, A. Kolmakov, A. J. Biacchi, T. A. Searles, A. R. Hight Walker, W. D. Rice, *Small* **2022**, *18*, 2105619.

[28] a) A. Baydin, N. Komatsu, F. Tay, S. Ghosh, T. Makihara, G. T. Noe, J. Kono, *Optica* **2021**, *8*, 760; b) K. Yanagi, R. Okada, Y. Ichinose, Y. Yomogida, F. Katsutani, W. Gao, J. Kono, *Nat. Commun.* **2018**, *9*, 1121; c) K.-C. Chiu, A. L. Falk, P.-H. Ho, D. B. Farmer, G. Tulevski, Y.-H. Lee, P. Avouris, S.-J. Han, *Nano Lett.* **2017**, *17*, 5641; d) W. Gao, C. F. Doiron, X. Li, J. Kono, G. V. Naik, *ACS Photonics* **2019**, *6*, 1602; e) S. Matano, H. Takahashi, N. Komatsu, Y. Shimura, K. Nakagawa, J. Kono, H. Maki, *ACS Mater. Lett.* **2022**, *4*, 626.

[29] a) F. Katsutani, W. Gao, X. Li, Y. Ichinose, Y. Yomogida, K. Yanagi, J. Kono, *Phys. Rev. B* **2019**, *99*, 035426; b) W. Gao, X. Li, M. Bamba, J. Kono, *Nat. Photonics* **2018**, *12*, 362.

[30] a) E. Iritani, N. Katagiri, T. Takenaka, Y. Yamashita, *Chem. Eng. Sci.* **2015**, *122*, 465; b) P. H. Hermans, H. L. Bredée, *Recl. Trav. Chim. Pays-Bas* **1935**, *54*, 680; c) V. E. Gonsalves, *Recl. Trav. Chim. Pays-Bas* **1950**, *69*, 873; d) H. P. Grace, *AIChE J.* **1956**, *2*, 307; e) J. Hermia, *Chem. Eng. Res. Des.* **1982**, *60*, 183; f) M. Hlavacek, F. Bouchet, *J. Membr. Sci.* **1993**, *82*, 285.

[31] a) B. Espinasse, P. Bacchin, P. Aimar, *Desalination* **2002**, *146*, 91; b) P. Bacchin, P. Aimar, R. W. Field, *J. Membr. Sci.* **2006**, *281*, 42; c) Y. Bessiere, N. Abidine, P. Bacchin, *J. Membr. Sci.* **2005**, *264*, 37.

[32] P. Bacchin, A. Marty, P. Duru, M. Meireles, P. Aimar, *Adv. Colloid Interface Sci.* **2011**, *164*, 2.

[33] E. M. Frohlich, J. L. Alonso, J. T. Borenstein, X. Zhang, M. A. Arnaout, J. L. Charest, *Lab Chip* **2013**, *13*, 2311.

[34] R. S. McLean, X. Huang, C. Khripin, A. Jagota, M. Zheng, *Nano Lett.* **2006**, *6*, 55.

[35] L. Wu, B. Gao, Y. Tian, R. Muñoz-Carpena, K. J. Zigler, *Langmuir* **2013**, *29*, 3976.

[36] a) J. Campo, S. Cambré, B. Botka, J. Obrzut, W. Wenseleers, J. A. Fagan, *ACS Nano* **2021**, *15*, 2301; b) J. Campo, Y. Piao, S. Lam, C. M. Stafford, J. K. Streit, J. R. Simpson, A. R. Hight Walker, J. A. Fagan, *Nanoscale Horiz.* **2016**, *1*, 317.

[37] a) J. A. Fagan, *Nanoscale Adv.* **2019**, *1*, 3307; b) H. Gui, J. K. Streit, J. A. Fagan, A. R. Hight Walker, C. Zhou, M. Zheng, *Nano Lett.* **2015**, *15*, 1642.

[38] C. Y. Khripin, X. Tu, J. M. Heddleston, C. Silvera-Batista, A. R. Hight Walker, J. Fagan, M. Zheng, *Anal. Chem.* **2013**, *85*, 1382.

[39] J. N. Israelachvili, *Intermolecular and surface forces*, Academic press, Amsterdam, Netherlands **2011**.

[40] J. S. Walker, Z. J. Macdermid, J. A. Fagan, A. Kolmakov, A. J. Biacchi, T. A. Searles, A. R. H. Walker, W. D. Rice, *Small* **2022**, *18*, 2105619.

[41] a) L. Onsager, *Ann. N. Y. Acad. Sci.* **1949**, *51*, 627; b) A. M. Donald, A. H. Windle, S. Hanna, *Liquid crystalline polymers*, Cambridge University Press, Cambridge, UK **2006**.

[42] V. A. Davis, L. M. Ericson, A. N. G. Parra-Vasquez, H. Fan, Y. Wang, V. Prieto, J. A. Longoria, S. Ramesh, R. K. Saini, C. Kittrell, W. E. Billups, W. W. Adams, R. H. Hauge, R. E. Smalley, M. Pasquali, *Macromolecules* **2004**, *37*, 154.

[43] J. P. F. Lagerwall, G. Scalia, *J. Mater. Chem.* **2008**, *18*, 2890.

[44] N. Fakhri, D. A. Tsyboulski, L. Cognet, R. B. Weisman, M. Pasquali, *Proc. Natl. Acad. Sci. USA* **2009**, *106*, 14219.

[45] G. B. van den Berg, C. A. Smolders, *J. Membr. Sci.* **1989**, *40*, 149.

[46] L. C. Liu, L. Moreno, I. Neretnieks, *Langmuir* **2009**, *25*, 679.

[47] a) P. Schuck, *Biophys. J.* **2000**, *78*, 1606; b) P. Schuck, *Sedimentation velocity analytical ultracentrifugation: discrete species and size-distributions of macromolecules and particles*, CRC Press, Boca Raton, USA **2016**.

[48] M. L. Mansfield, J. F. Douglas, *Macromolecules* **2008**, *41*, 5422.

[49] C. A. Silvera Batista, M. Zheng, C. Y. Khripin, X. Tu, J. A. Fagan, *Langmuir* **2014**, *30*, 4895.